Chinese Chemical Letters 37 (2026) 111510

Contents lists available at ScienceDirect

Chinese Chemical Letters

journal homepage: www.elsevier.com/locate/cclet

Computer-aided discovery of peptidyl arginine deiminase 4 inhibitors to suppress NETosis and accelerate diabetic wound healing

Huijuan Luo[a,1], Haiyue Zuo[b,1], Jianzhong Zhu[a,c,1], Juanjuan Zhao[b], Roufen Chen[d], Xinle Yang[d], Fangqi Cao[a], Ruohan Lou[a], Xiaowu Dong[d], Yangyang Bian[b,*], Ligen Lin[a,e,*]

[a] State Key Laboratory of Mechanism and Quality of Chinese Medicine, Institute of Chinese Medical Sciences, University of Macau, Macau 999078, China
[b] Key Laboratory of Resource Biology and Modern Biotechnology in Western China, College of Life Science, Northwest University, Xi'an 710069, China
[c] Department of Drug Design and Pharmacology, Faculty of Health and Medical Sciences, University of Copenhagen, Copenhagen DK-2100, Denmark
[d] College of Pharmaceutical Sciences, Zhejiang University, Hangzhou 310058, China
[e] Department of Pharmaceutical Sciences, Faculty of Health Sciences, University of Macau, Macau 999078, China

ARTICLE INFO

Article history:
Received 7 May 2025
Revised 20 June 2025
Accepted 25 June 2025
Available online 25 June 2025

Keywords:
Peptidyl arginine deiminase 4
Molecular docking and molecular dynamics
Neutrophil extracellular traps
Gliquidone
Diabetic wound healing

ABSTRACT

Neutrophil extracellular traps (NETs) are a significant unfavorable factor for wound healing in diabetes. Citrullination of histone by peptidyl arginine deiminase 4 (PAD4) is the prerequisite for NETs formation. Therefore, PAD4 inhibitors are a promising NETs-targeting strategy to accelerate diabetic wound healing. Herein, a virtual screening workflow incorporating molecular docking and molecular dynamics was performed on a library of U.S. Food and Drug Administration (FDA)-approved drugs, resulting in the identification of gliquidone as a new PAD4 inhibitor. Gliquidone binds directly to PAD4, inhibits its activity, and interrupts NETs formation in neutrophils, which in turn rescues functional impairment in fibroblasts. Furthermore, in streptozotocin-induced diabetic mice, gliquidone accelerates wound healing. Taken together, gliquidone was successfully identified as a new PAD4 inhibitor through a computer-aided virtual screening pipeline, which might be a therapeutic agent against diabetic foot ulcers.

© 2026 Published by Elsevier B.V. on behalf of Chinese Chemical Society and Institute of Materia Medica, Chinese Academy of Medical Sciences.

Neutrophils, as one of the foremost guards of host defense, are the main leukocytes involved in innate immunity to phagocytose and kill pathogens by releasing neutrophil extracellular traps (NETs) [1]. NETs are mushroom-like structures of DNA fibers coated with histone, antimicrobial peptides, and proteases such as neutrophil elastase, cathepsin G, and myeloperoxidase (MPO) [1,2]. The citrullination of arginine residues of histones by peptidyl arginine deiminase 4 (PAD4) is the prerequisite for NETs releasing (NETosis), which initiates massive chromatin decondensation [3,4]. Both clinical and experimental evidence has shown that PAD4 is involved in aberrant levels of NETs [5]. The expression of PAD4 was increased in neutrophils from diabetic patients, and the diabetic microenvironment predisposed neutrophils to NETosis with higher levels of citrullinated histone H3 (CitH3) in diabetic wounds and thus impaired wound closure [6,7]. In contrast, disruption of NETs in PAD4 knockout mice facilitated wound healing [7–9], suggesting that PAD4 inhibitors might be encouraging therapeutics for the treatment of diabetic foot ulcers. PAD4 inhibitors can be classified into reversible and irreversible categories, which were designed based on structural simulations of the active sites of PAD4. A great proportion of PAD4 inhibitors are amidine derivatives. Cl-amidine is a first-generation irreversible PAD4 inhibitor targeting the catalytic cysteine residue, with the half maximal inhibitory concentration (IC_{50}) value of 6 μmol/L. Unfortunately, Cl-amidine also inhibits PAD1/3/4, and its bioavailability and pharmacokinetic properties are poor [10]. GSK484, a benzimidazole derivative, is a reversible PAD4 inhibitor with relatively high selectivity and nanomolar inhibitory activity (IC_{50}: 200 nmol/L (without Ca^{2+}), 1 μmol/L (with Ca^{2+})). GSK484 still has partial cross-inhibition against PAD2 and lacks sufficient *in vivo* pharmacological validation [11]. JBI-1044, a structural analog of GSK484 with an IC_{50} value of 102 nmol/L, is a PAD4 inhibitor in the Investigational New Drug stage [12]. Till now, most studies on PAD4 inhibitors remain in the experimental or preclinical stage, there is no approved PAD4 inhibitor in the clinic. Therefore, there is an urgent need to discover novel PAD4 inhibitors that demonstrate dual attributes of high selectivity and optimized pharmacological profiles encompassing both safety and therapeutic efficacy.

Virtual screening has emerged as a powerful computational strategy in drug discovery. By leveraging either structure-based or

* Corresponding authors.
E-mail addresses: bianyy@nwu.edu.cn (Y. Bian), ligenl@um.edu.mo (L. Lin).
[1] These authors contributed equally to this work.

https://doi.org/10.1016/j.cclet.2025.111510
1001-8417/© 2026 Published by Elsevier B.V. on behalf of Chinese Chemical Society and Institute of Materia Medica, Chinese Academy of Medical Sciences.

ligand-based approaches, virtual screening prioritizes molecules with a high likelihood of binding to a given biological target. Among structure-based techniques, molecular docking plays a central role by predicting the most favorable binding conformations and interaction energies between small molecules and the target protein. However, docking alone often provides a static snapshot of ligand-protein interactions, necessitating molecular dynamics simulations to account for the conformational flexibility of biomolecules and solvent effects, thereby refining binding predictions and improving hit selection [13]. Such computational approaches have been employed to screen inhibitors to a cascade of protein targets, including wound healing-related prolyl hydroxylase 2 inhibitor [14], diagnosis of wound healing [15], cancer-related histone deacetylase 2 inhibitors [16], and butyrylcholinesterase inhibitor for Alzheimer's disease treatment [17].

Drug repurposing, also known as drug repositioning, has gained significant attention as a cost-effective and time-efficient strategy for identifying new therapeutic applications of existing drugs due to established safety profiles and thereby accelerating the transition to clinical trials. Computational approaches, particularly those integrating virtual screening, such as molecular docking and molecular dynamics simulations, have proven invaluable in systematically evaluating approved or investigational drugs against new targets. For example, efforts have been made in applying them to repurpose approved drugs for targeting pathogenic virus superfamily 1 helicase [18], cancer treatment [19], and rare diseases [20].

Herein, a computational pipeline that sequentially incorporating molecular docking and molecular dynamics was performed to discover new PAD4 inhibitors from U.S. Food and Drug Administration (FDA)-approved drugs. As a result, gliquidone (Gli), a sulfonylureas-type oral medication to treat type 2 diabetes through primarily stimulating pancreatic insulin release, was found to bind directly to PAD4, disrupt NETs, and accelerate diabetic wound healing.

A total of 2470 FDA-approved drugs were initially docked with PAD4 protein (PDB: 4X8C) using Libdock, and the top 100 molecules were subsequently docked with PAD4 protein using CDOCKER. The top five drugs, as scored by CDOCKER, were selected for binding energy calculations using molecular dynamics. Among these, DB03310 and DB00183 demonstrated higher binding affinity than GSK484 (Tables S1 and S2, Figs. S1 and S2 in Supporting information). These two drugs were then tested for their PAD4 inhibitory activity. However, they showed no dose-dependent inhibition against PAD4 and did not reduce the level of NETosis in dHL-60 cells (Fig. S3 in Supporting information). Following this initial setback, we conducted a second round of docking using AutoDock Vina for the 100 molecules from Libdock. Fifteen drugs were identified with scores equivalent to or better than GSK484 (Fig. S4a in Supporting information). To increase the chance of discovering positive hits, we expanded our selection to include all 15 drugs and omitted the computationally intensive molecular dynamics studies due to the large number of compounds. Eight drugs were commercially available and tested for their PAD4 inhibitory activity (Table S3 in Supporting information). The assay results revealed that three drugs (DB01167, DB00681, and DB01251) exhibited significant PAD4 inhibitory activities; among them, DB01251 (gliquidone, Gli) displayed 77.31 % potency of GSK484 at the same concentration (Fig. S4b in Supporting information). Notably, Gli was one of the two common drugs identified by both CDOCKER and AutoDock Vina from the list of compounds that were calculated as better inhibitors than GSK484 (Fig. 1a and Table S4 in Supporting information). Gli was found to orient similarly to GSK484 within the binding pocket (Fig. 1b) and maintained some similar interactions as GSK484, namely hydrophobic interactions with P584 at the heterocycle terminal, and with V643, A581, and E474 at the phenyl group. In addition, the sulfonyl-urea linkage

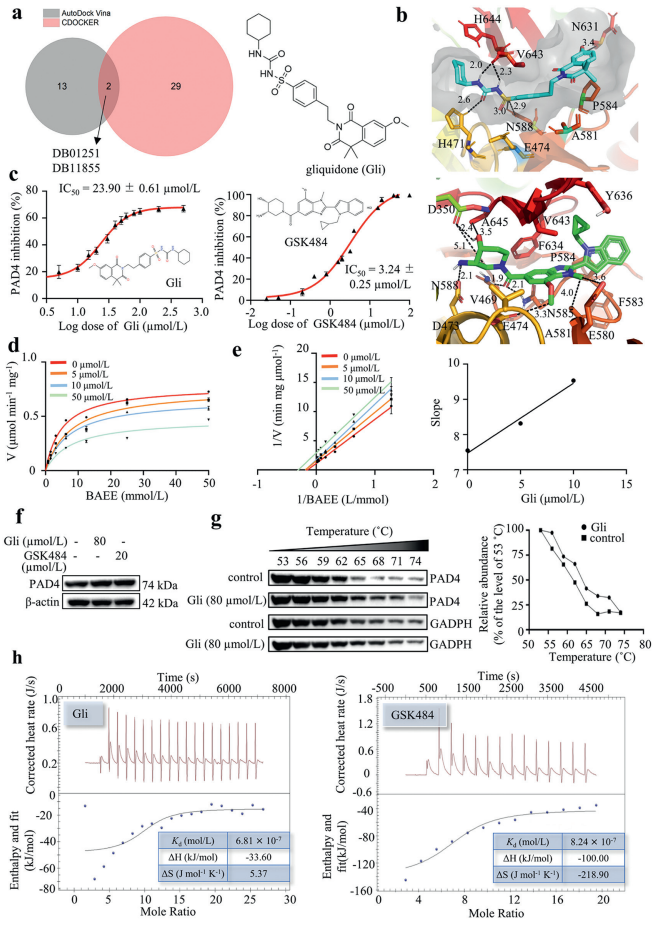


Fig. 1. Identification of gliquidone as a new PAD4 inhibitor *via* virtual screening. (a) Venn diagram showing the common hits evaluated by CDOCKER and AutoDock Vina, and the chemical structure of Gli. (b) Non-bond interactions between DB01251 (Gli), GSK484, and PAD4 were analyzed by Discovery Studio Visualizer. Black dashed lines represent hydrogen bonds with values expressed in angstroms. The grey surface indicates the pocket of PAD4. (c) The PAD4 inhibitory activity of Gli and GSK484. (d) Michaelis-Menten plots at varying Gli concentrations (0–50 μmol/L). (e) Lineweaver-Burk plots showing mixed inhibition patterns, and slope replot confirming the concentration-dependent inhibition. (f) The expression of PAD4 in dHL-60 cells treated with or without Gli. β-Actin was used as a loading control. (g) CETSA was performed on dHL-60 cells treated with or without Gli. GAPDH, glyceraldehyde 3-phosphate dehydrogenase. (h) ITC analysis of the interaction between the PAD4 protein and Gli (left) or GSK484 (right). Upper panel: raw heat signals; lower panel: integrated binding isotherm. Data represented means ± SD ($n = 3$).

was anchored by five conventional hydrogen bonds with N588, V643, and H471. The cyclohexanyl group at the other terminal formed hydrophobic interactions with H644 and H471. Overall, Gli mimicked the interactions with PAD4 observed for GSK484. To explore the structural basis of PAD4 inhibition and validate docking predictions, we further performed a comparative analysis of Gli and four sulfonylurea analogs, including gliclazide, glimepiride (Amaryl), glipizide (Glucotrol) and glyburide. These compounds share a common sulfonylurea core but differ in their hydrophobic and aromatic substituents. Gli showed the strongest binding affinity (−10.334 kcal/mol) among the five sulfonylurea analogs, underpinned by its optimal balance of the combination of extensive hydrogen bonding, aromatic stacking, and bulky hydrophobic groups, (Figs. S5 and S6, Table S5 in Supporting information). Based on these findings, Gli was chosen for further studies.

Using benzoyl-arginine ethyl ester (BAEE) as the substrate of citrullination, Gli was assayed for its PAD4 inhibitory effect. The result showed that Gli inhibited PAD4 activity in a dose-dependent manner with an IC_{50} value of 23.90 ± 0.61 μmol/L, which is compa-

rable with the positive control GSK484 ($IC_{50} = 3.24 \pm 0.25$ μmol/L, Fig. 1c). Next, the inhibition kinetic of Gli against PAD4 was carefully investigated by the classical COLDER method, with BAEE as the substrate. Inhibition kinetic behavior was studied according to the Michaelis-Menten equation with different concentrations of Gli and substrate. In the absence of Gli, the K_m and V_{max} values were 5.09 mmol/L and 0.78 μmol min^{-1} mg^{-1} protein (Fig. 1d). When the added concentration of Gli was in the range of 0–50 μmol/L, the K_m gradually increased with the increase of the compound concentration (from 5.09 mmol/L to 7.94 mmol/L), and the corresponding V_{max} significantly decreased (from 0.78 μmol min^{-1} mg^{-1} to 0.48 μmol min^{-1} mg^{-1}). Furthermore, the Lineweaver-Burk plot and its corresponding slope plot were drawn (Fig. 1e). These results indicated that Gli may inhibit PAD4 activity in a mixed mode including noncompetitive and uncompetitive manners [11,21].

After being treated with Gli (80 μmol/L) or GSK484 (20 μmol/L), the dHL-60 cells exhibited no obvious change in the protein expression of PAD4 when compared with the control group (Fig. 1f). Cellular thermal shift assay (CETSA) was performed to verify whether Gli could interact directly with PAD4 as molecular modeling suggested. Compared with the vehicle control (DMSO), Gli treatment obviously stabilized PAD4 at various temperatures from 53 °C to 74 °C, suggesting that Gli bound directly to PAD4 to increase the thermal stability (Fig. 1g). To further confirm the interaction of compounds with PAD4, isothermal titration calorimetry (ITC) assay was performed. As expected, GSK484 showed a dissociation constant ($K_d = 8.24 \times 10^{-7}$ mol/L) similar to Gli ($K_d = 6.81 \times 10^{-7}$ mol/L), indicating the similar high affinity with the Gli (Fig. 1h). The above evidence indicated that Gli might bind PAD4 to inhibit its activity, but not influence its expression.

To further validate the effect of Gli on NETosis, HL-60 cells were differentiated into neutrophil-like cells by DMSO or all-trans retinoic acid (ATRA) [22]. The neutrophil surface marker, CD11b, was used to evaluate the differentiation efficiency of HL-60 cells. It was observed that CD11b expression was significantly higher in the DMSO–dHL-60 cells than that in the ATRA-dHL-60 cells (Fig. S7a in Supporting information). Therefore, DMSO was chosen to induce differentiation of HL-60 cells into neutrophil-like cells. Subsequently, the cytotoxicity of Gli in dHL-60 cells was evaluated, and the results showed that Gli did not exhibit cytotoxicity in dHL-60 cells up to 120 μmol/L, nor did GSK484 (Fig. S7b in Supporting information).

The NETs formation involves histone citrullination, chromatin decondensation, and extracellular release of decondensed chromatin, producing cell-free DNA (cfDNA), MPO, and CitH3. To explore the effect of Gli on NETosis, the level of cfDNA was determined by Sytox Green staining. The results showed that calcium ionophore treatment increased the content of cfDNA, whereas Gli significantly reduced the level of cfDNA in calcium ionophore-stimulated dHL-60 cells (Fig. 2a). Furthermore, the nuclei stained by Sytox Green and Hoechst 33342 were decondensed in dHL-60 cells treated with calcium ionophore compared with the normal control, which was obviously reversed by Gli treatment (Fig. 2b). The CitH3 expression in calcium ionophore-induced dHL-60 cells was significantly increased, and either Gli or GSK484 effectively suppressed CitH3 expression in dHL-60 cells (Fig. 2c), which was further supported by the immunofluorescence staining of CitH3 (Fig. 2d). Moreover, Gli treatment reduced the expression of MPO in calcium ionophore-induced dHL-60 cells (Fig. 2e). Taken together, Gli interrupts calcium ionophore-induced NETosis in dHL-60 cells.

In diabetic wounds and high-glucose environments, excessive NETs formation by activated neutrophils impairs the function of fibroblasts and delays wound healing [23]. Thus, we explored the role of Gli in the function of fibroblasts in this context. dHL-60 cells were treated with or without Gli and GSK484 (positive

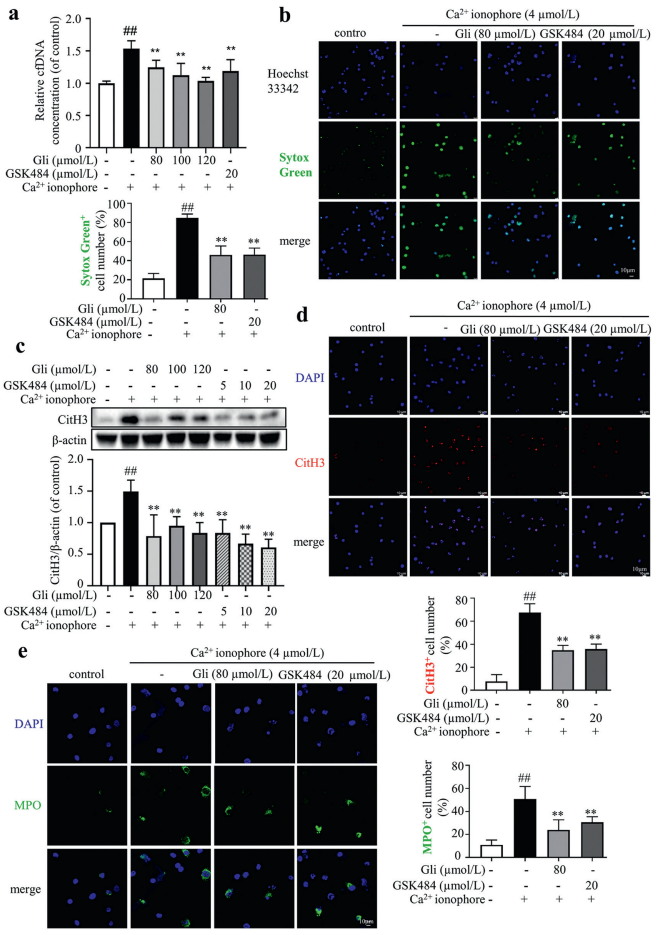


Fig. 2. Gliquidone effectively suppressed calcium ionophore-induced NETosis in dHL-60 cells. (a) Gli reduced the content of cfDNA in calcium ionophore-induced dHL-60 cells. (b) Immunofluorescence staining of Sytox Green and Hoechst 33342 to visualize cfDNA release. Scale bar: 10 μm. (c) Gli reduced CitH3 expression in calcium ionophore-induced dHL-60 cells. β-Actin was used as a loading control. Immunofluorescence image of CitH3 (d, scale bar: 10 μm) and MPO (e, scale bar: 25 μm). Data represented means ± SD ($n = 3$). $^{\#\#}P < 0.01$ *vs.* vehicle control. $^{*}P < 0.05$, $^{**}P < 0.01$ *vs.* calcium ionophore-induced group. DAPI, 4′,6-diamidino-2-phenylindole.

control). Subsequently, NETs were extracted from each group, and added in the culture medium of BJ fibroblasts. The results of cell counting kit-8 (CCK8) and 5-ethynyl-2′-deoxyuridine (EdU) assays showed that, compared with the control group, treatment of NETs derived from calcium ionophore-treated dHL-60 cells significantly impaired the proliferation of BJ fibroblasts, in contrast, treatment of NETs extracted from Gli- or GSK484-treated dHL-60 cells exhibited a pronounced proliferation capacity, comparable with that of the control group (Figs. 3a and b). Next, the transwell and cell scratch assays were performed to assess the migration ability of BJ fibroblasts. As expected, treatment of NETs from calcium ionophore-induced dHL-60 cells hindered fibroblast migration, which was almost abolished by Gli or GSK484 treatment (Figs. 3c and d). Overall, these findings suggested that Gli rescued the impaired function of fibroblasts through reducing NETs formation in neutrophils.

Next, the effect of Gli in accelerating wound healing was evaluated in normal control (NC) mice and STZ-induced diabetic mice (DM). All animal care and experimental procedures were consistent with the guidelines and regulations, and were approved by the Animal Ethical and Welfare Committee of the University of Macau (No. UMARE-033–2017). Due to temperature sensitivity and well

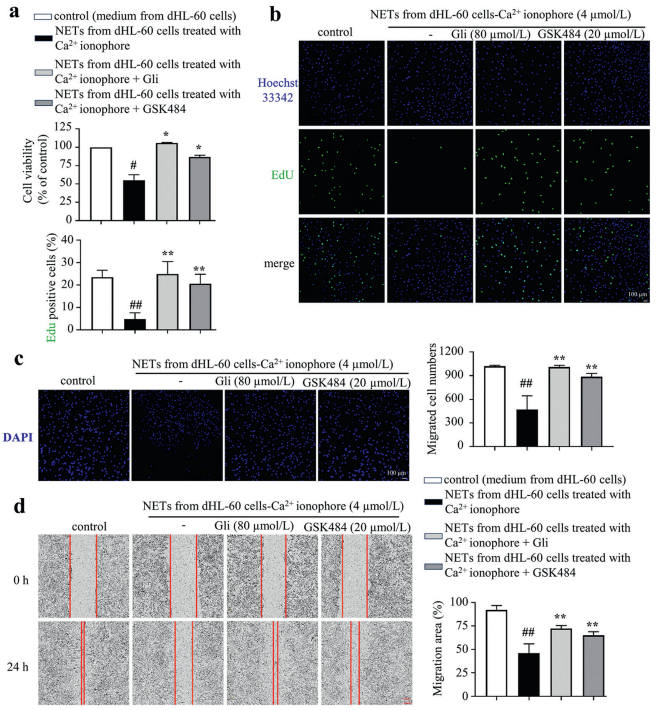


Fig. 3. Gliquidone attenuates NETs-induced functional impairment in fibroblasts. CCK8 (a) and EdU (b) assays were performed to evaluate the proliferation of BJ fibroblasts treated with or without NETs extracted from dHL-60 cells. EdU, green; DAPI, blue. Scale bar: 100 μm. The migration ability of fibroblasts treated with or without NETs extracted from different groups of dHL-60 cells, assessed by transwell assay (c, scale bar: 100 μm) and cell scratch assay (d, scale bar: 200 μm). DAPI, blue. Data represented means ± SD ($n = 3$). $^{\#}P < 0.05$, $^{\#\#}P < 0.01$ *vs.* control; $^{*}P < 0.05$, $^{**}P < 0.01$ *vs.* NETs from dHL-60 cells treated with calcium ionophore group.

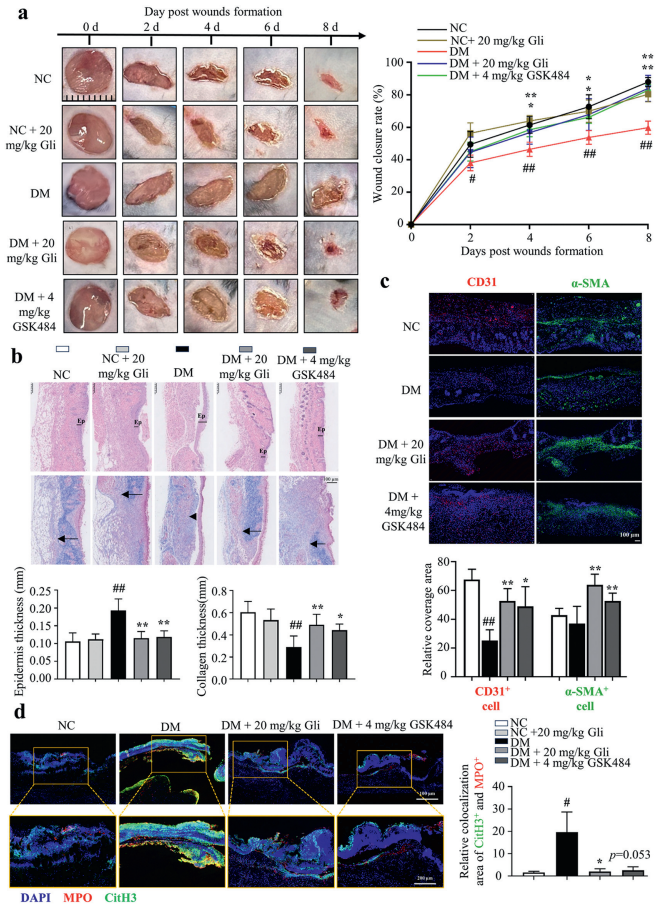


Fig. 4. Gliquidone-loaded hydrogel accelerates wound healing in diabetic mice *via* suppressing NETs formation. (a) Representative images of wound areas (left) and wound closure rates (right). (b) Representative images of H&E staining (up) and Masson's trichrome staining (down) of dorsal skin section. Ep: epidermis; black arrow: collagen thickness. (c) Immunofluorescence staining images of CD31 (red) and α-SMA (green) in the wound tissues of mice on 8 days post-injury. Scale bar: 100 μm. (d) Immunofluorescence staining images of CitH3 and MPO in wounds on 3 days post-injury ($n = 5$). CitH3, green; MPO, red; DAPI, blue. Scale bar: 100 μm (up), 200 μm (down). Data are expressed as the mean ± SD ($n = 5$). $^{\#}P < 0.05$, $^{\#\#}P < 0.01$ *vs.* NC; $^{*}P < 0.05$, $^{**}P < 0.01$ *vs.* DM.

adhesiveness on the skin, pluronic F-127 was chosen to prepare the hydrogel. Two full-thickness skin lesions were excised in the interscapular area of each animal and locally treated with a hydrogel-loaded vehicle, Gli or GSK484, once a day for 8 days (Fig. S8 in Supporting information). The wound images were captured every other day to monitor the wound healing process, and wound closure rates were calculated for each group. Representative images of the wound area in each group were taken on days 0, 2, 4, 6, and 8 post-wounding (Fig. 4a). Compared to the NC mice, the healing of wounds was obviously interrupted in DM mice (Fig. 4a). On 2, 4, 6 and 8 days post-injury, the DM group of mice exhibited 38%, 46%, 53% and 59% wound closure, the DM mice treated with 20 mg/kg Gli showed 45%, 57%, 68% and 84% wound closure, and DM mice treated with 4 mg/kg GSK484 displayed 45%, 58%, 66% and 83% wound closure, respectively (Fig. 4a). However, 20 mg/kg Gli treatment did not speed up wound closure in NC mice (Fig. 4a). Collectively, these findings demonstrate that Gli accelerates the healing process of diabetic wounds, while exhibiting no significant impact on the healing of non-diabetic wounds. The histologic structure change of the regenerated dermis was analyzed on wound tissues collected on day 8 using hematoxylin & eosin (H&E) staining and Masson's trichrome staining. The H&E staining results revealed that Gli administration markedly attenuated epidermal hyperplasia compared to DM mice (Fig. 4b). Additionally, Gli treatment increased the collagen deposition in wound areas compared to the DM group (Fig. 4b). The immunofluorescence staining of CD31 showed that compared to the DM, Gli or GSK484 administration exhibited an obviously higher density of $CD31^{+}$ microvessel in the diabetic wound areas (Fig. 4c). Subsequently, the immunofluorescence staining of α-smooth muscle actin (α-SMA) revealed the expression level of α-SMA was decreased in wounds from DM mice, indicating fewer fibroblasts differentiated into contractile myofibroblasts; while treatment of Gli or GSK484 obviously increased α-SMA expression level (Fig. 4c). Interestingly, compared to the DM mice, the expression level of α-SMA in NC group was comparable, which may be attributed to accelerated wound healing progression in NC mice. In normal wound healing, myofibroblast apoptosis gradually reduces the α-SMA expression to prevent excessive collagen fibre contraction and scar tissue formation [24]. Taken together, these results indicated that Gli enhanced collagen disposition and promoted angiogenesis to accelerate wound healing in diabetic mice.

To verify whether Gli promotes diabetic wound healing *via* suppression of NETs formation, PAD4, CitH3 and MPO expression levels (NETs formation marker) and serum cfDNA level were evaluated on day 3 post-injury. The Western blots showed that the CitH3 expression was significantly increased in wounds from DM mice, and either Gli or GSK484 treatment effectively suppressed CitH3 expression (Fig. S9a in Supporting information). In DM mice, the PAD4 expression was upregulated in wounds, while neither Gli nor GSK484 treatment affect PAD4 expression (Fig. S9a). Moreover, the serum levels of cfDNA in DM mice were decreased by Gli or GSK484 treatment (Fig. S9b in Supporting information). The infiltration and activation of neutrophils in wound tissues

were determined *via* the immunofluorescence labelling of Ly6G (a neutrophil surface marker) and MPO (mostly expressed in neutrophils), respectively. The results revealed that DM mice exhibited pronounced neutrophil infiltration and activation in wounds; notably, either Gli or GSK484 treatment markedly reversed the changes (Fig. S9c in Supporting information). Furthermore, the immunofluorescence staining images showed that Gli or GSK484 treatment greatly reduced the co-localization areas of $CitH3^{+}$ and MPO^{+} in wounds, compared to the DM group (Fig. 4d), indicating the over-produced NETs in the DM mice was abolished by Gli or GSK484 treatment. Collectively, these results indicated that Gli suppressed NETs formation to promote the remodelling phase of chronic wound closure, thus contributing to diabetic wound healing acceleration.

Taken together, Gli was identified as a novel PAD4 inhibitor through a computer-aided virtual screening pipeline, which interrupts NETs formation in neutrophils, rescues functional impairment in fibroblasts, and accelerates wound healing in diabetic mice. Encouragingly, Gli has been approved by the FDA as an antidiabetic drug, which might be applied as a therapeutic agent for diabetic foot ulcers.

Declaration of competing interest

The authors declare that they have no known competing financial interests or personal relationships that could have appeared to influence the work reported in this paper.

CRediT authorship contribution statement

Huijuan Luo: Writing – original draft, Methodology, Investigation, Formal analysis. **Haiyue Zuo:** Writing – review & editing, Software, Methodology, Investigation, Data curation. **Jianzhong Zhu:** Writing – review & editing, Software, Methodology, Investigation, Formal analysis, Conceptualization. **Juanjuan Zhao:** Visualization, Methodology, Investigation. **Roufen Chen:** Writing – review & editing, Validation, Methodology, Investigation. **Xinle Yang:** Writing – review & editing, Validation, Methodology, Investigation. **Fangqi Cao:** Writing – review & editing, Visualization, Validation, Investigation. **Ruohan Lou:** Writing – review & editing, Visualization, Methodology, Data curation. **Xiaowu Dong:** Writing – review & editing, Validation, Supervision, Methodology, Data curation. **Yangyang Bian:** Writing – review & editing, Supervision, Resources, Funding acquisition, Data curation. **Ligen Lin:** Writing – review & editing, Validation, Supervision, Project administration, Funding acquisition, Data curation, Conceptualization.

Acknowledgments

This work was supported by National Natural Science Foundation of China (Nos. 82073715, 22274130), the Science and Technology Development Fund, Macao SAR (Nos. FDCT 0001/2021/AKP, FDCT 005/2023/SKL), the Hong Kong/Macao Joint Research and Development Fund Project of Wuyi University (No. 2022WGALH15), and the Key Research and Development Program of Shaanxi (No. 2023-BSF-322).

Supplementary materials

Supplementary material associated with this article can be found, in the online version, at doi:10.1016/j.cclet.2025.111510.

References

[1] V. Brinkmann, U. Reichard, C. Goosmann, et al., Science 303 (2004) 1532–1535.
[2] V. Papayannopoulos, Nat. Rev. Immunol. 18 (2018) 134–147.
[3] S.L. Wong, D.D. Wagner, FASEB J. 32 (2018) 6258–6370.
[4] M. Leshner, S. Wang, C. Lewis, et al., Front. Immunol. 3 (2012) 307.
[5] P. Li, M. Li, M.R. Lindberg, et al., J. Exp. Med. 207 (2010) 1853–1862.
[6] Z. Zhu, S. Zhou, S. Li, et al., Trends Pharmacol. Sci. 45 (2024) 1033–1045.
[7] S.L. Wong, M. Demers, K. Martinod, et al., Nat. Med. 21 (2015) 815–819.
[8] L. Kang, H. Yu, X. Yang, et al., Nat. Commun. 11 (2020) 2488.
[9] C.T. Yang, L. Chen, W.L. Chen, et al., Mol. Cell. Endocrinol. 480 (2019) 74–82.
[10] D. Zhu, Y. Lu, Y. Wang, et al., Pharmaceutics 14 (2022) 2414.
[11] H.D. Lewis, J. Liddle, J.E. Coote, et al., Nat. Chem. Biol. 11 (2015) 189–191.
[12] S.G. Aiken, T. Grimes, S. Munro, et al., Expert Opin. Ther. Pat. 35 (2025) 611–621.
[13] Z. Wang, H. Sun, C. Shen, et al., Phys. Chem. Chem. Phys. 22 (2020) 3149–3159.
[14] J. Zhu, C. Chen, J. Dong, et al., Chin. Chem. Lett. 34 (2023) 107514.
[15] J. Deng, G. Shi, Z. Ye, et al., Chin. Chem. Lett. 36 (2025) 110496.
[16] A. Shah, A. Choudhary, M. Jain, et al., 3 Biotech 14 (2024) 83.
[17] Q. Zhang, Y. Li, Q. Jin, et al., Chin. Chem. Lett. 37 (2026) 110964.
[18] Z. Li, Y. Ding, J. Hu, et al., Chin. Chem. Lett. 36 (2025) 110737.
[19] Y. Xia, M. Sun, H. Huang, et al., Signal Transduct. Target. Ther. 9 (2024) 92.
[20] H.I. Roessler, N.V.A.M. Knoers, M.M. van Haelst, et al., Trends Pharmacol. Sci. 42 (2021) 255–267.
[21] J. Gao, M. Zhou, D. Chen, et al., Food Chem. 422 (2023) 136179.
[22] A. Manda-Handzlik, W. Bystrzycka, M. Wachowska, et al., Immunol. Cell Biol. 96 (2018) 413–425.
[23] Z. Chu, Q. Huang, K. Ma, et al., Bioact. Mater. 27 (2023) 257–270.
[24] S. Mascharak, H.E. desJardins-Park, M.F. Davitt, et al., Science 372 (2021) eaba2374.